Geohazard Mechanics 3 (2025) 87–98

Contents lists available at ScienceDirect

Geohazard Mechanics

journal homepage: www.keaipublishing.com/en/journals/geohazard-mechanics

Kinetic characterisation of sandstone exposed to high temperature-water cooling cycle treatments under the impact loading: from the perspective of geohazard

Lei Hong [a], Wen Wang [a,b,*], Xuewen Cao [c], Yuxiang Song [a], XiaoWei Lu [d], Shu Jiang [e], Cheng Zhai [d]

[a] College of Energy Science and Engineering, Henan University of Science and Technology, Jiaozuo, 454003, China
[b] Provincial Collaborative Innovation Centre for Safe Production and Clean and Efficient Utilisation of Coal, Jiaozuo, 454000, China
[c] College of Resources and Civil Engineering, Northeastern University, Shenyang, 110819, China
[d] School of Safety Engineering, China University of Mining and Technology, Xuzhou, 221116, China
[e] School of Earth Resources, China University of Geosciences, Wuhan, 430074, China

ARTICLE INFO

Keywords:
High-temperature-water cooling cycle
Sandstone
Kinetic characterisation
Crack extension
Energy dissipation
Well collapses

ABSTRACT

Enhanced Geothermal Systems (EGS) improve geothermal energy extraction but can rapidly cool high-temperature rocks, leading to internal fractures that weaken mechanical properties and pose risks such as well collapses and seismic events. Understanding the physico-mechanical changes in dry hot rocks, particularly sandstone, when high-temperature water cooling cycles is essential. This study examines the dynamic behavior of sandstone through impact tests at varying temperatures and cycles. Results show that as temperature and cycle count increased, peak dynamic stress decreased while dynamic strain increased. A critical temperature range of 500–600 °C was identified, beyond which significant changes in dynamic stress and strain occurred, indicating severe damage to the specimens' stability. High-temperature water cooling cycles enhanced energy reflectivity and dissipated energy, reducing transmittance. The study revealed that between 200 and 400 °C, tensile damage predominated, while between 500 and 600 °C, compression-shear damage was dominant. Increasing temperature and cycles led to more extensive cracking and increased rock fragmentation. These findings provide a basis for assessing the stability of sandstone and offer theoretical insights into mechanical properties, energy transfer, and crack propagation in geothermal energy extraction, aiding in the prevention of geological disasters.

1. Introduction

Geothermal energy, particularly from deep dry hot rock (DHR) formations, presents a significant opportunity for sustainable energy production. However, the low permeability of these formations poses challenges to traditional extraction methods, which rely on dual-well systems composed of injection and production wells. These methods often exhibit inefficiencies and elevated energy consumption. To address these limitations, Enhanced Geothermal Systems (EGS) have been developed, employing artificial fracturing to improve rock permeability. While this innovation enhances extraction efficiency, it introduces new complications, notably the rapid cooling of high-temperature rocks due to water injection [1–3]. This sudden temperature change triggers thermal cycling, which induces internal fractures within the rock mass. Over time, these fractures weaken the mechanical properties of the rock, heightening the risk of secondary hazards such as wellbore collapse and induced seismicity, both of which jeopardize the operational safety of geothermal plants.

China possesses abundant geothermal resources, particularly in the northwest, north, and northeast regions, where sedimentary basin-type DHR formations are prevalent. These formations are characterized by deep, high-temperature, low-permeability rock structures that lack internal water, necessitating artificial water injection and fracturing to create geothermal reservoirs. During the extraction process, the rocks are exposed to repeated high-temperature-water cooling cycles, which significantly alter their physical and mechanical properties. These changes can compromise the stability of the extraction process, leading to safety concerns and reduced operational efficiency. Historical examples,

* Corresponding author. College of Energy Science and Engineering, Henan University of Science and Technology, Jiaozuo, 454003, China.
E-mail address: wangwen2006@hpu.edu.cn (W. Wang).

https://doi.org/10.1016/j.ghm.2024.12.001
Received 14 December 2023; Received in revised form 13 October 2024; Accepted 4 December 2024
Available online 30 December 2024

such as the induced seismicity at the Basel EGS project in Switzerland and the Pohang project in South Korea, underscore the severity of these risks. Both projects experienced induced earthquakes that caused substantial structural damage, ultimately leading to the suspension of operations.

Given these risks, it is essential to investigate the dynamic behavior of rocks under high-temperature-water cooling cycles to improve the safety and sustainability of geothermal extraction. A deeper understanding of the mechanisms driving rock degradation under these conditions will enable the optimization of extraction technologies, support more accurate risk assessments, and provide a foundation for developing mitigation strategies to prevent geological hazards.

The study of the dynamic behavior of sandstone exposed to high-temperature-water cooling cycle treatments, particularly under impact loading, remains relatively limited. Existing research primarily focuses on how different cooling methods influence the physical and mechanical properties of rocks. Kumari et al. [4,5] through examining the mechanical behavior of granite after natural cooling and water cooling post-high-temperature exposure, found that water cooling caused more severe thermal damage, especially when temperatures exceeded 400 °C. Similarly, Wang et al. [6] demonstrated that water cooling exacerbated the degradation of rock properties following high temperatures, particularly at elevated temperature ranges. Liang et al. [7] further revealed that increased porosity induced by high temperatures led to a direct decline in the mechanical performance of sandstone. Huang et al. [8] discovered that the attenuation coefficient of parameters such as peak strength did not monotonically increase and decrease with temperature and high-temperature inflection points when the temperature of high-temperature marble cooled by water was higher than 400 °C.

In studies addressing the effects of high-temperature-water cooling cycles, Yin et al. [9] highlighted the significant impact of cyclic heating and cooling on the crack propagation behavior in rocks, uncovering the mechanisms of crack initiation and extension. Yu et al. [10] investigated how repeated high-temperature-water cooling treatments affect the physical and mechanical properties of granite, finding that both the number of cycles and heating temperature played a critical role in the degree of damage. Li et al. [11] further explored the relationship between thermal crack deterioration mechanisms, heating temperature, and cycle frequency in granite. Wang et al. [12] performed the mechanical experiments on granite under temperature-humidity cycling conditions. Through analysis of its deformation and damage characteristics, they proposed that the maximum tensile strain of circular granite could serve as the basis for damage determination.

Regarding the dynamic behavior of rocks under impact loading, Yin et al. [13] used the Split-Hopkinson Pressure Bar (SHPB) apparatus to conduct dynamic compression tests on sandstone after high-temperature treatment, and found that the dynamic peak strength of sandstone gradually decreased with rising temperatures, accompanied by increased fragmentation. Yu et al. [14] conducted cyclic impact experiments under different confining pressures. Through damage factor analysis, they found that sandstone's damage factor grew with the mean strain rate in a power function. Li et al. [15] confirmed the similar findings, highlighting the damage evolution in granite under repeated impact conditions. Lin et al. [16] examined marble under impact loading and discovered the effects of impact velocity and confining pressure on damage severity, providing a foundation for understanding the damage evolution in sandstone under impact loads.

From an energy perspective, studies by Ping et al. [17] and Dai et al. [18] demonstrated that the energy absorption capacity of rocks decreased progressively during cyclic impact, with energy absorption being closely tied to impact conditions such as velocity and loading mode. Zhu et al. [19] conducted impact experiments on high-temperature granite using the SHPB, and proposed a damage model based on changes in energy absorption, providing a theoretical basis for understanding the damage mechanisms of rocks under dynamic conditions following high-temperature-water cooling cycles. Wang et al. [20] investigated the energy dissipation characteristics of weathered red sandstone under varied axial pressures and impact velocities. Zhang et al. [21] carried out the impact compression experiments on coal. By examining fragmentary energy consumption and block size distributions, they discovered relationships between the coal's fractal dimension and energy dissipation density.

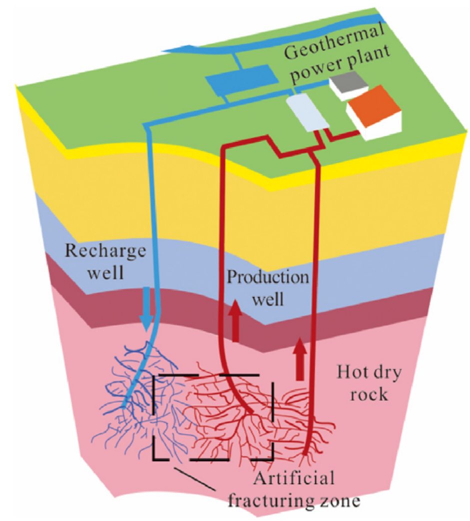

Fig. 1. Schematic diagram of hot dry rock mining.

However, most current research focuses on static loading or single-impact conditions, with limited exploration of the dynamic behavior of sandstone subjected to complex impact loads after high-temperature-water cooling cycles, particularly in geohazard-related scenarios. Further in-depth research in this area will contribute to a better understanding of the failure mechanisms of sandstone in extreme environmental conditions, offering critical insights for disaster prevention and mitigation.

2. Sample preparation and experimental programme

2.1. Specimen preparation

Sandstone was selected as the research object for the experiment, with blocks sourced from Shaanxi Province in two batches. These blocks were greyish-white and lacked obvious joints. According to international rock mechanics testing standards, the blocks were processed into Φ50 mm × 100 mm cylinders for static load test specimens and Φ50mm × 50 mm cylinders for dynamic load test specimens, totaling 120 pieces. To ensure test accuracy, the non-parallelism and non-perpendicularity of the specimen surfaces were maintained within 0.02 mm, as shown in Fig. 2.

High-temperature treatment was conducted using a KSW-5D-12 box-type resistance furnace, which includes heating elements and temperature controllers (see Fig. 3). The heating rate was approximately 5 °C/min up to a maximum temperature of 1200 °C, as depicted in Fig. 1. Specimen heating temperatures were set at five levels: 200, 300, 400, 500, and 600 °C. At each temperature, four groups underwent 1, 3, 5, and 7 high-temperature-water cooling cycles respectively, with three specimens per cycle serving as the control group, totaling 60 specimens.

The high temperature-water cooling cycle test process was as follows:

(1) High-temperature treatment: Specimens were dried and then placed into the resistance furnace using crucible tongs, held at the set temperature for 4 h after the furnace reached the preset temperature;
(2) Specimen mass measurement: Using crucible clamps, specimens were removed from the furnace and placed on an electronic scale for mass measurement. This quick process resulted in minimal high-temperature specimen cooling;

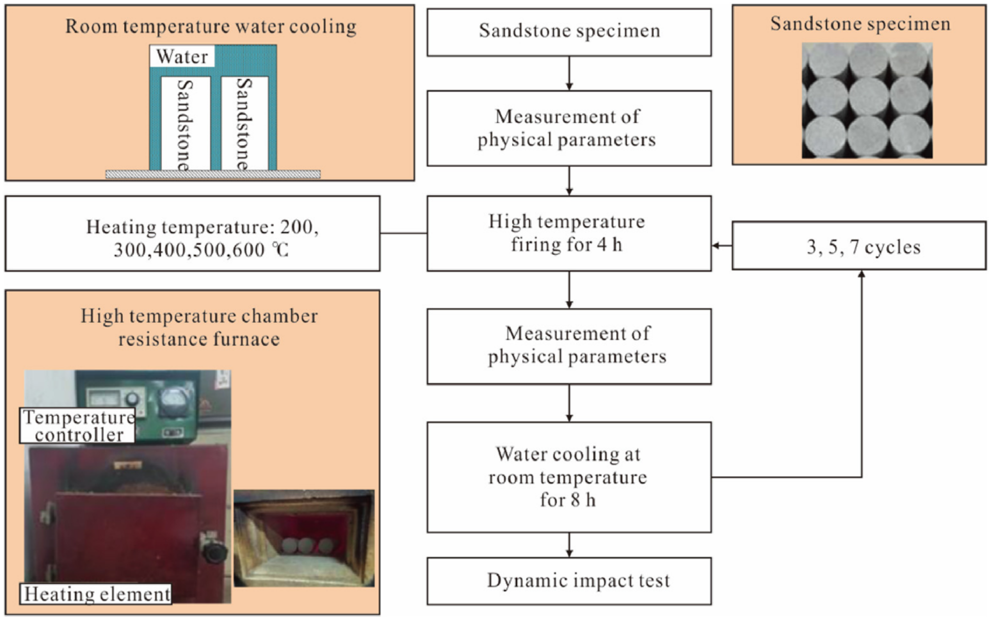

Fig. 2. Test flow chart.

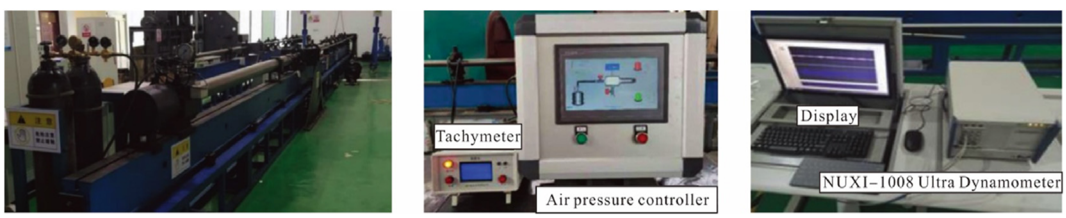

Fig. 3. Hopkinson impact test system composition.

Table 1
Main technical indicators of Hopkinson impact test.

Functionality	Single axis dynamic load shock	Maximum pressure in axial direction	40 MPa
Bullet velocity	50 m/s	Length of bullets	600 mm
Diameter of rod	50 mm	Maximum working pressure	10 MPa

(3) Water cooling: Weighed specimens were placed in room temperature water for 8 h to cool down to room temperature;
(4) Cycle recurrence: Sandstone specimens undergoing high temperature-water cooling cycles repeated the above three steps for each cycle.

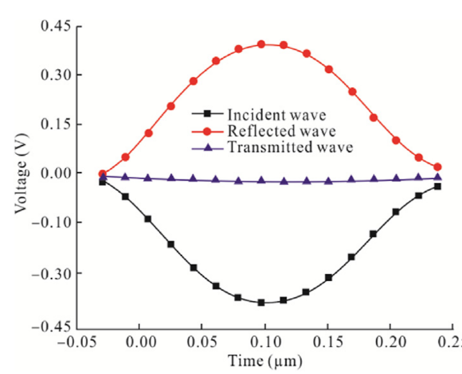

Fig. 5. Equilibrium verification of sandstone samples.

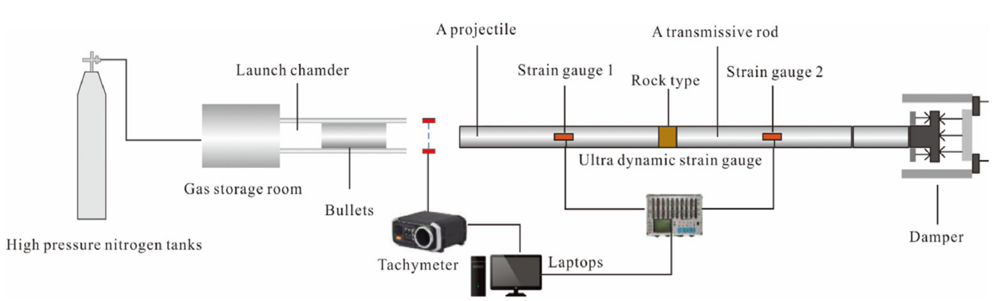

Fig. 4. Schematic diagram of dynamic loading of sandstone.

Multiple cycles simulated the physical and mechanical changes of high-temperature rock specimens under repetitive water exposure. The cycle test flow chart is provided in Fig. 2.

2.2. Introduction to the test equipment

The dynamic load impact tests utilized a Hopkinson impact system from Henan University of Science and Technology, consisting of a launching system, control system, and signal collection system.

Before testing, the positions of the incident and transmission rods and the buffer device were debugged. The bullet was pushed deep into the launch cavity. The tachymeter and high-speed camera were set up and positioned. Specimens were placed, and the data acquisition system was opened to check impact waveform data. After confirming no issues, data was saved. The Hopkinson impact system is shown in Fig. 2, with working parameters listed in Table 1.

2.3. Dynamic load experiment programme

After high temperature-water cooling cycles, the sandstone specimens were divided into five groups at 200, 300, 400, 500, and 600 °C. Each temperature group had four subsets with 1, 3, 5, and 7 cycles. Specimen ends were evenly coated with butter, then placed between the incident and transmission rods, pressed into tight contact to reduce test errors. Specimens were covered with transparent plastic boxes to control debris and recorded by the high-speed camera. The impact velocity was set at 10 m/s.

Fig. 4 shows the dynamic impact test loading of sandstone after high temperature-water cooling cycle. A velocimeter is arranged between the launching cavity and the incident rod to measure the impact velocity of the bullet. In addition, strain gauges are set at equal distances between the incident rod and the transmission rod near the end of the specimen, and a hyper dynamic strain gauge and a computer are used to collect and store the data. In the dynamic load test, the bullet affects the incident rod with a certain speed. Then in this process, the strain gauge 1 on the incident rod collects the incident strain ε_I, and the stress wave is transmitted into the rock sample from the incident rod, and the reflection occurs at the contact surface between the incident rod and the rock sample, generating the reflection strain ε_R, which is measured by the strain gauges on the incident rod 1. Then, the stress wave is transmitted into the transmitting rod, and the transmitting strain ε_T generated by the end of the transmitting rod is measured by the strain gauges on the transmitting rod 2, which is measured by the strain gauge on the transmitting rod. The transmitted strain ε_T at the end of the transmitting rod is measured by the strain gauge 2 on the transmitting rod.

Fig. 4 shows the dynamic impact test loading of sandstone after high-temperature water cooling cycles. A velocimeter is set between the launching cavity and the incident rod to measure the impact velocity of the bullet, while strain gauges are evenly spaced between the incident rod and the transmission rod near the specimen's end. A hyperdynamic strain gauge and a computer are used to collect and store the data. In the dynamic load test, the bullet impacts the incident rod at a certain speed. During this process, the strain gauge on the incident rod collects the incident strain ε_I. The stress wave is transmitted into the rock sample from the incident rod, and reflection occurs at the contact surface between the incident rod and the rock sample, generating the reflection strain ε_R, which is measured by the strain gauges on the incident rod. The stress wave is then transmitted into the transmitting rod, and the transmitted strain ε_T generated by the end of the transmitting rod is measured by the strain gauges on the transmitting rod.

Table 2
Peak dynamic load strength and strain of sandstone samples.

Processing temperature (°C)	Number of cycles	Peak dynamic stress (MPa)	Peak dynamic strain
200	1	159.7	0.00592
	3	156.9	0.00617
	5	154.8	0.00646
	7	154.1	0.00692
300	1	159.0	0.00613
	3	156.8	0.00636
	5	152.7	0.00665
	7	152.1	0.00711
400	1	157.6	0.00627
	3	154.1	0.00643
	5	152.8	0.00695
	7	150.3	0.007
500	1	157.9	0.00679
	3	154.1	0.0069
	5	149.3	0.0072
	7	141.3	0.00745
600	1	152.4	0.00812
	3	98.5	0.01019
	5	93.0	0.01169
	7	87.9	0.01261

3. Dynamic load mechanical characteristics of sandstone under high temperature-water cooling cycle conditions

3.1. Dynamic strength characterisation

3.1.1. SHPB data processing method

Based on the two-wave method for data analysis, equilibrium validation can be conducted using voltage signals. According to the equilibrium condition, the sum of the incident and reflected waves should be approximately equal to the transmitted wave, i.e., $V_i + V_r \approx V_t$. During validation, plot $(V_i + V_r)$ and V_t as functions of time and perform a quantitative comparison. If the two curves overlap or the difference is small during the loading phase, it indicates that the specimen has reached the equilibrium during the experiment. Based on the above analysis, the equilibrium verification is shown in Fig. 5.

The one-dimensional SHPB (Split Hopkinson Pressure Bar) testing technique relies on the assumptions of "one-dimensional stress wave in the rod" and "specimen stress/strain homogenisation". These assumptions imply that there is stress equilibrium or homogeneous deformation of the specimen during dynamic impact loading. The average stress σ, strain ε, and strain rate $\dot{\varepsilon}$ can be determined using the following equations [22–24]:

$$\sigma(t) = \frac{[\sigma_I(t) - \sigma_R(t) + \sigma_T(t)]A_e}{(2A_S)} \tag{1}$$

$$\varepsilon(t) = \frac{1}{\rho_e C_e L_e} \int_0^t [\sigma_I(t) - \sigma_R(t) + \sigma_T(t)]dt \tag{2}$$

$$\dot{\varepsilon}(t) = \frac{1}{\rho_e C_e L_s} [\sigma_I(t) - \sigma_R(t) + \sigma_T(t)] \tag{3}$$

where $\sigma_I t$, σ_R(t), and σ_T(t) are the incident, reflected, and transmitted stresses at time t, respectively. The incident and transmitted stresses are considered to be positive for compressive stresses, while reflected stresses are positive for tensile stresses. $\rho_e C_e$ is the wave impedance of the elastic rod; A_e and A_s are the cross-sectional areas of the elastic rod and the sample, respectively; and L_s is the length of the specimen.

3.1.2. Analysis of dynamic stress and strain changes with the number of cycles

For the dynamic load tests on sandstone specimens under high temperature-water cooling cyclic conditions, bullet velocity was the quantitative measure with specimen heating temperature and cooling cycle number as the variables. Testing occurred in groups. By analyzing the dynamic load test results of sandstone specimens at the same temperature but with differing cycle numbers, peak dynamic stresses and strains were obtained as shown in Table 2. Based on the test findings,

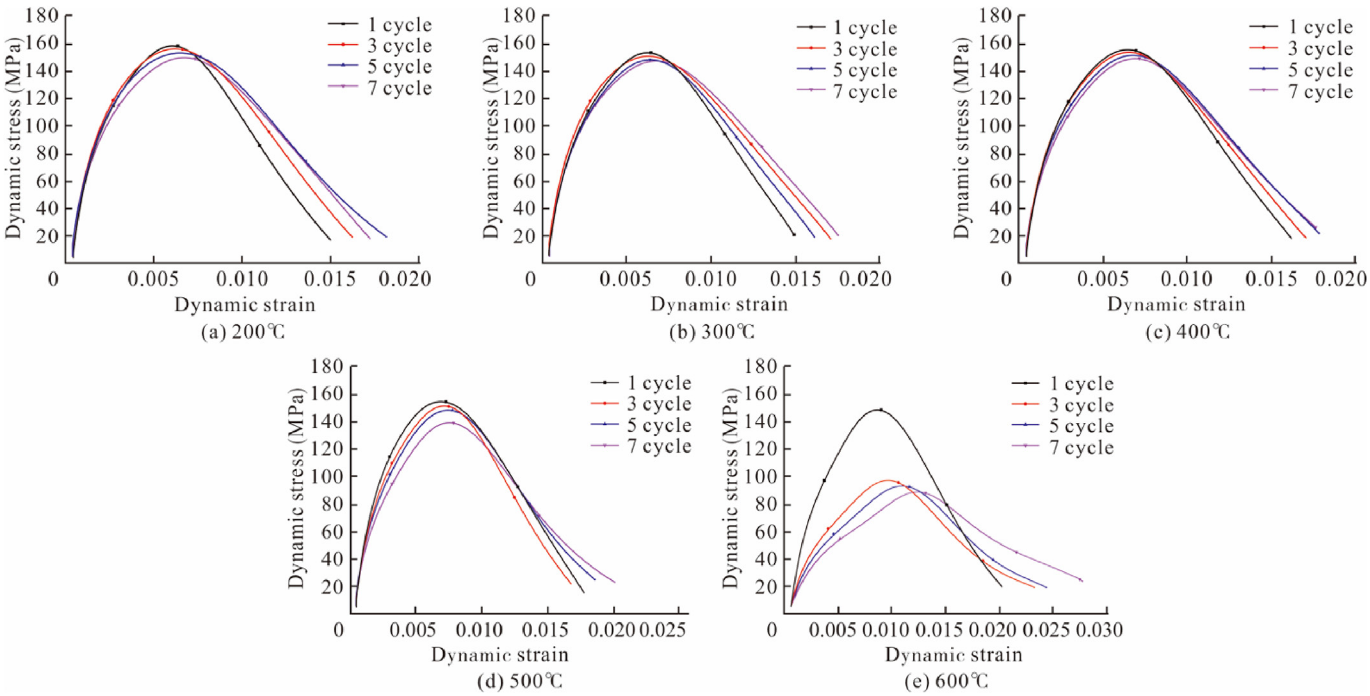

Fig. 6. Dynamic stress-strain curve with temperature change.

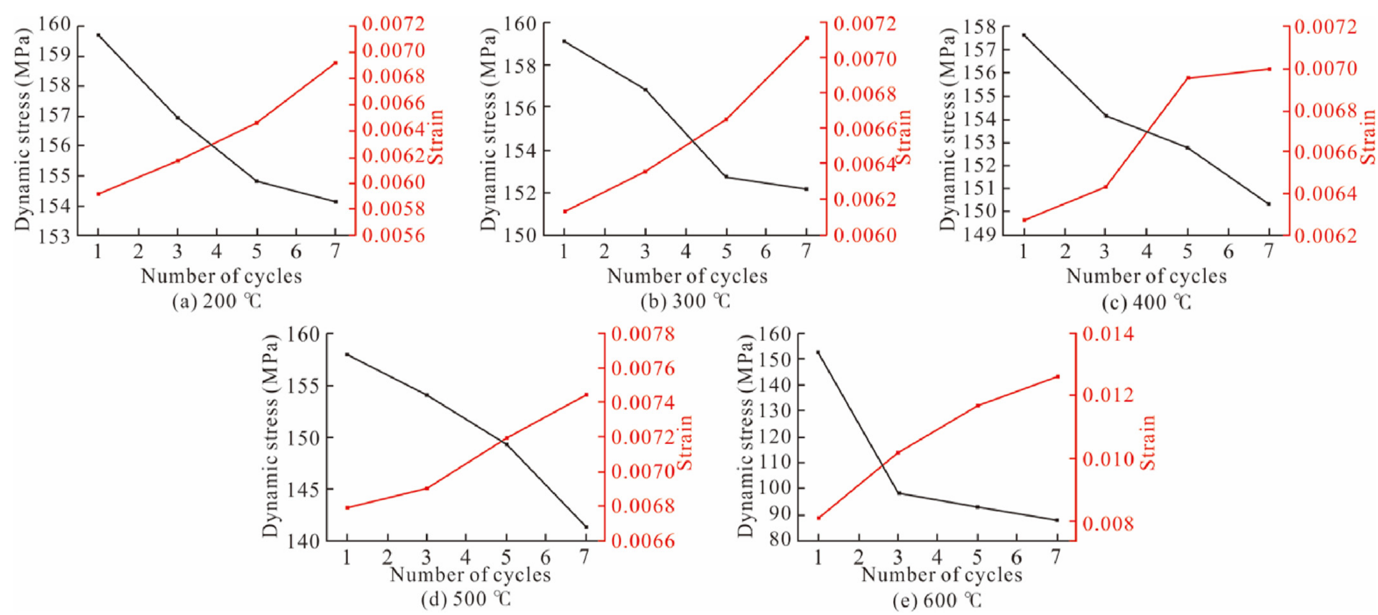

Fig. 7. Dynamic stress-strain variation curve with temperature change.

dynamic stress-strain curves of high temperature-water cooled sandstone were plotted. Relationship curves between specimen dynamic peak stress and strain vs. cycle number were generated as displayed in Figs. 6 and 7.

Fig. 6 shows that the specimen peak dynamic stress decreases and dynamic strain increases with more cycles. After 1 cycle at 200 °C, the peak dynamic stress was 159 MPa, which gradually reduced to 154 MPa after 7 cycles, a total decrease of 3.4%. At 300 °C, the peak stress decreased from 159 to 152 MPa, representing a 4.3% drop. At 400 °C, the peak stress fell from 157 to 150 MPa, indicating a 4.6% decrease. At 500 °C, it decreased from 157 to 141 MPa (a 10.5% reduction), and at 600 °C, from 152 to 87 MPa (a 42.3% decrease). The dynamic stress clearly diminishes with more cycles, with greater stress reduction at higher temperatures. From 200 to 400 °C, reductions ranged from 3.4% to 4.6%, while at 500 °C, it was 10.5%. At 600 °C, the 42.3% sudden increase signifies an intensified decline.

After 1 cycle at 200 °C, the peak dynamic strain was 0.0059, rising to 0.0069 after 7 cycles—a 16.9% increase. At 300 °C, strain grew from 0.0061 to 0.0071 (a 16.0% increase) and at 400 °C, from 0.0062 to 0.007 (an 11.6% increase). At 500 °C, it increased from 0.0067 to 0.0074 (a 9.7% increase), and at 600 °C, from 0.0081 to 0.0126 (a 55.3% increase). Though strains increase with more cycles at every temperature, growth rates decrease with higher temperatures across 7 cycles (from 16.8% at 200 °C down to 9.7% at 500 °C). However, notably at 600 °C, the growth suddenly spikes to 55.2%.

The analysis indicates a critical temperature between 500 and 600 °C influencing sandstone's dynamic properties after high temperature-water

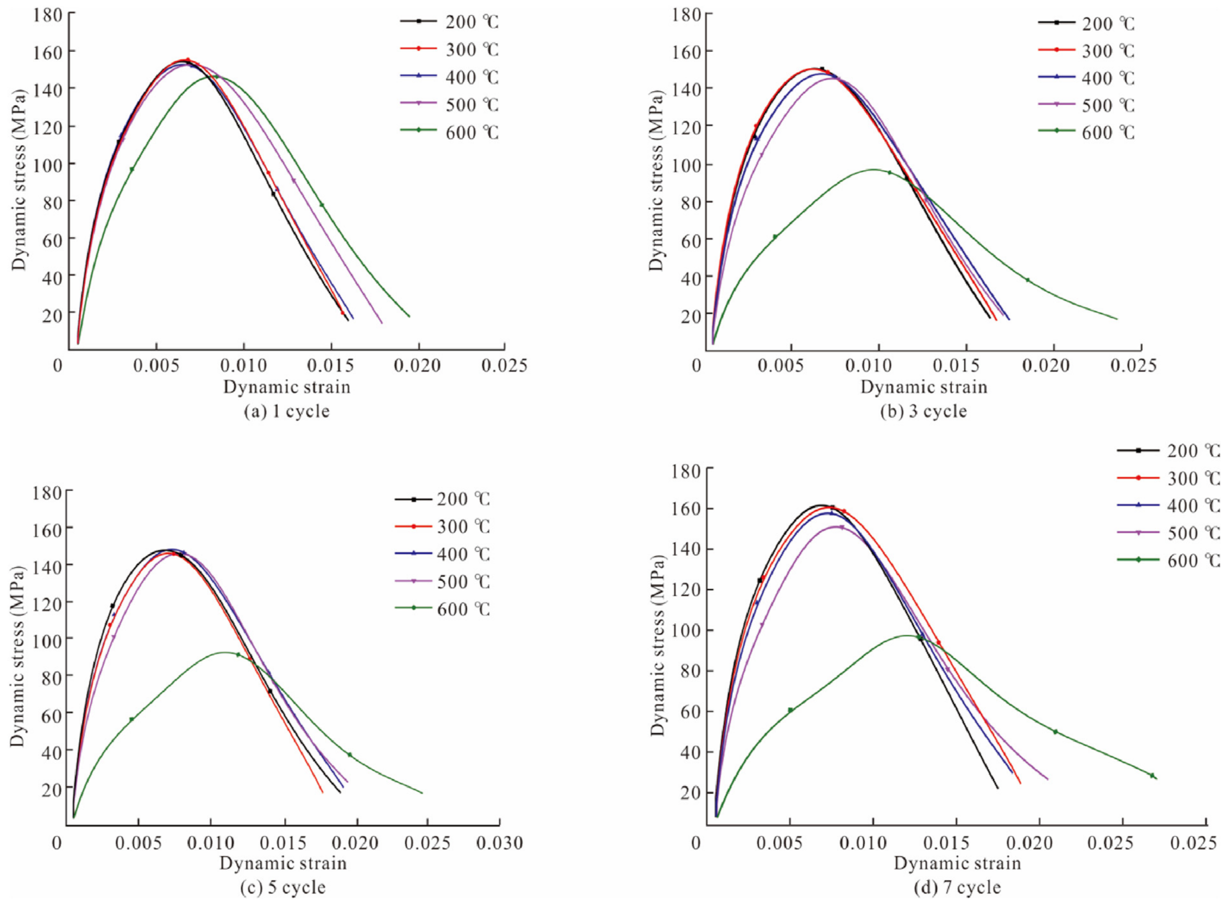

Fig. 8. Dynamic stress-strain curve with the number of cycles.

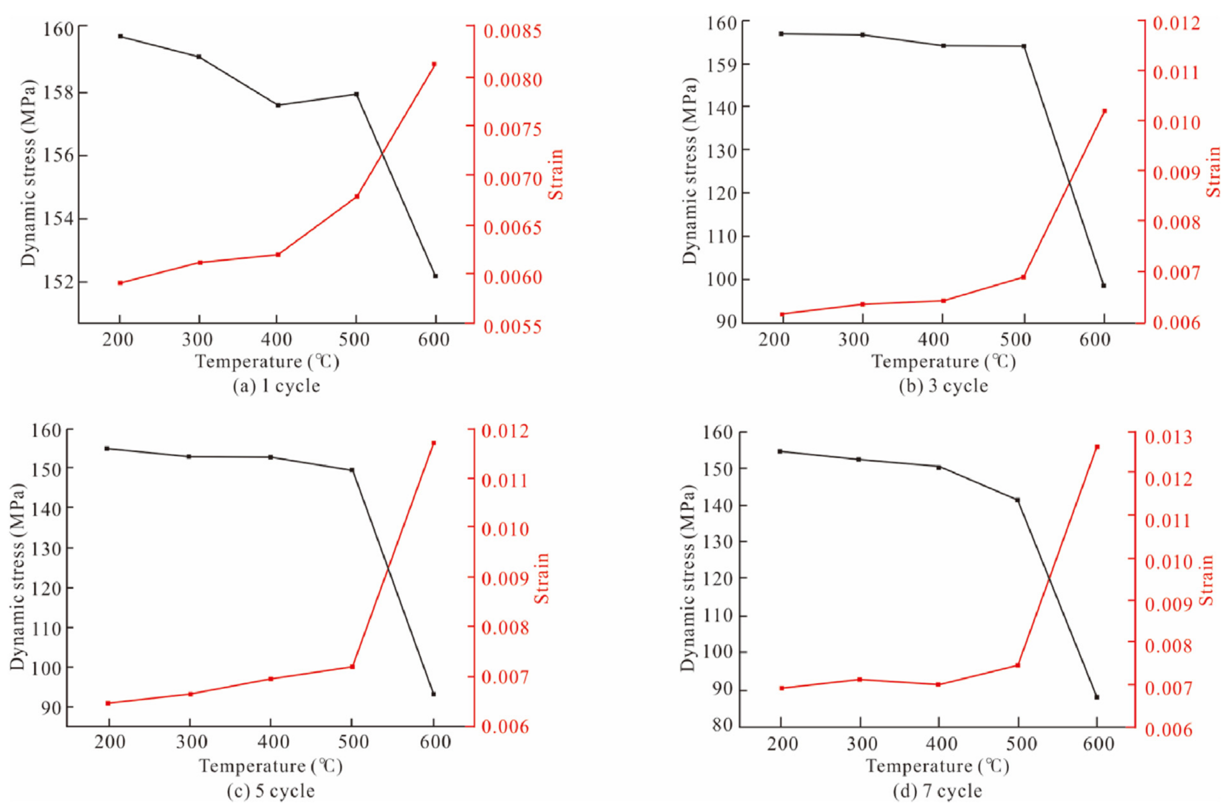

Fig. 9. Dynamic stress-strain variation curve with the number of cycles.

Table 3
Energy change of sandstone under dynamic load.

Specimen number	E_I (J)	E_R (J)	E_T (J)	E_a	η_r	η_t	η_a
200–1	738.66	305.07	161.03	272.57	0.413	0.218	0.369
200–3	745.44	310.10	157.29	278.05	0.416	0.211	0.373
200–5	765.26	319.88	157.64	287.74	0.418	0.206	0.376
200–7	756.08	316.04	154.24	285.80	0.418	0.204	0.377
300–1	764.18	315.61	165.83	282.74	0.413	0.217	0.370
300–3	758.52	315.54	160.05	282.93	0.416	0.211	0.373
300–5	803.61	337.52	160.72	305.37	0.420	0.200	0.380
300–7	731.58	307.99	145.58	278.01	0.421	0.199	0.380
400–1	774.07	321.24	164.88	287.95	0.415	0.213	0.372
400–3	771.63	322.54	157.41	291.68	0.418	0.204	0.378
400–5	765.61	321.56	153.89	290.16	0.420	0.201	0.379
400–7	737.33	311.15	143.78	282.40	0.422	0.195	0.383
500–1	800.33	332.14	171.27	296.92	0.415	0.214	0.371
500–3	736.25	307.75	150.19	278.31	0.418	0.204	0.378
500–5	803.77	340.00	154.32	309.45	0.423	0.192	0.385
500–7	751.04	323.70	129.18	298.16	0.431	0.172	0.397
600–1	782.06	329.25	154.85	297.96	0.421	0.198	0.381
600–3	734.17	346.53	52.13	355.51	0.472	0.071	0.457
600–5	758.48	363.31	44.75	350.42	0.479	0.059	0.462
600–7	791.57	380.75	38.00	372.82	0.481	0.048	0.471

cooling cycles. Below this threshold, under impact loads, specimen peak dynamic stresses steadily decrease but drop rates rise gradually. Above it, stresses rapidly plunge as peak strengths dramatically weaken, signaling weakened impact deformation resistance and serious temperature-induced sandstone damage. This threshold also governs specimen strain—while strains gradually grow with temperature rise, growth rates decline until abruptly soaring past this point. Thus, sandstone resistance to deformation is seriously impaired above the critical point with substantial damage. Greater cycles and heating worsen the specimen strength and deformation via heightened thermal-moisture stresses over material cohesion strengths, with cycling compounding rock damage.

3.1.2.1. Analysis of dynamic stress and strain with temperature change.- Dynamic stress-strain curves were plotted for sandstone specimens undergoing the same cooling cycles but at varied temperatures. Relationships among the dynamic peak stress, strain, and heating temperature were also graphed as shown in Figs. 8 and 9.

As seen in Fig. 7, the peak dynamic stress of the sandstone specimen shows a decreasing trend with the increase of heating temperature, while the dynamic strain shows an increasing trend. After 1 cycle, the peak dynamic stress of the 200 °C specimen was 159 MPa, and with the increase of temperature to 600 °C, the peak dynamic stress gradually decreased to 152 MPa, with a total stress decrease of 4.5%. After 3 cycles, the peak stress of the specimen was reduced from 156 to 98 MPa, a decrease of 37.2%. After 5 cycles, the peak stress was reduced from 155 to 93 MPa, a 39.9% decrease. After 7 cycles, the peak stress decreased from 154 to 88 MPa, a 43% decrease.

There are two types of decreasing trends:

(1) Slow decreasing trend: After 1 cycle, the specimen stress changes minimally. For specimens tested after 1 cycle at temperatures ranging from 200 to 600 °C, the dynamic stress decreased by 7.2 MPa, a reduction rate of 4.1%, indicating that the effect of temperature on specimen strength after 1 cycle is small.
(2) Rapid decline trend: After 3 to 7 cycles, the stress reduction magnitude increases significantly with temperature. The stress reduction sizes for specimens after 3, 5, and 7 cycles were 58.4, 61.7, and 66.2 MPa, respectively, with reduction rates of 37.1%, 39%, and 42.2%.

After 1 cycle, the peak dynamic strain of the specimen at 200 °C was 0.0059. As the heating temperature increased to 600 °C, the dynamic strain of the specimen increased to 0.0081, a total increase of 37.1%. After 3 cycles, the strain increased from 0.0061 to 0.0101, a 65.1% increase. After 5 cycles, the strain increased from 0.0064 to 0.0116, an 80.9% increase. After 7 cycles, the strain increased from 0.0069 to 0.0126, an 82.2% increase.

There are two stages of specimen strain change:

(1) Stage 1: 200–500 °C. The strain steadily increases, with a maximum strain increase of 8.2% between adjacent temperatures under the same number of cycles, indicating that below 500 °C, temperature has less impact on specimen strain;
(2) Stage 2: 500–600 °C: The strain rises sharply, with the smallest increase of 37.1% after 1 cycle and an 82.2% increase after 7 cycles. This indicates that a temperature range between 500 and 600 °C significantly affects the stability of sandstone under dynamic load impact.

3.2. Characterisation of energy changes

3.2.1. Energy calculation method and energy calculation results

In the dynamic load test, when a specimen is impacted, the energy of each part of the impact loading process can be calculated using the following formulas, according to the law of conservation of energy [25]:

$$E_I = \frac{A_e}{\rho_e C_e}\int_0^T \sigma_I^2(t)dt \tag{4}$$

$$E_R = \frac{A_e}{\rho_e C_e}\int_0^T \sigma_R^2(t)dt \tag{5}$$

$$E_T = \frac{A_e}{\rho_e C_e}\int_0^T \sigma_T^2(t)dt \tag{6}$$

$$E_a = E_I - E_R - E_T \tag{7}$$

where ρ_e is the density of the elastic rod;C_e is the wave speed in the elastic rod; A_e is the cross-sectional area of the elastic rod; $\sigma_I(t)$, $\sigma_R(t)$, and $\sigma_T(t)$ are the incident, reflected, and transmitted stresses at time; and E_I, E_R, E_T, and E_a are the incident, reflected, transmitted, and absorbed energies, respectively.

Considering the relationship between incident energy and bullet speed, the introduction of energy reflectivity (η_r), energy transmittance (η_t), and energy dissipation rate (η_a) helps eliminate errors caused by variations in bullet speed. This approach offers a more intuitive understanding of the energy changes in the specimen under different temperatures and cycle durations.

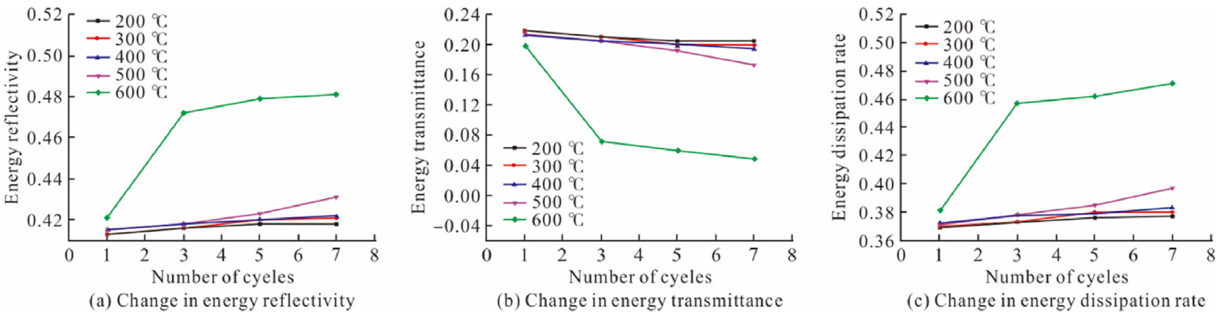

Fig. 10. Change of energy rate for different cycles at the same temperature.

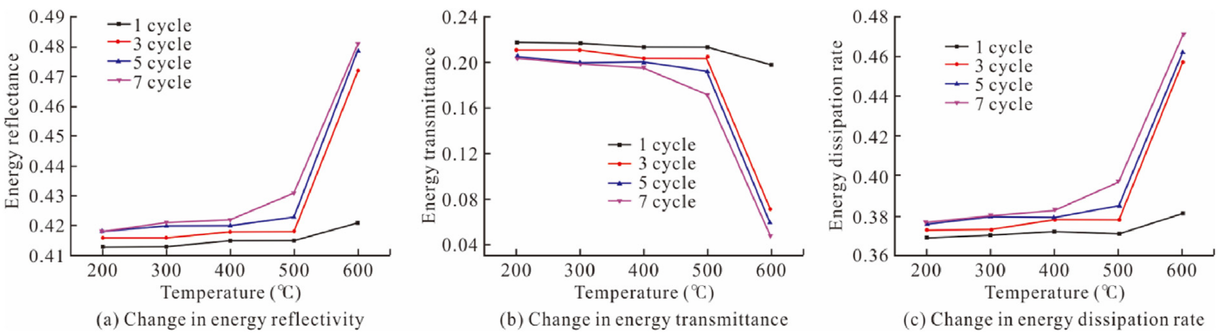

Fig. 11. Rate of energy change at different temperatures for the same number of cycles.

The following equations are used for calculation:

$$\eta_a = \frac{E_a}{E_I} = \frac{\dfrac{A_e}{\rho_e C_e}\displaystyle\int_0^T \left[\sigma_I^2(t) - \sigma_R^2(t) - \sigma_T^2(t)\right] dt}{\dfrac{A_e}{\rho_e C_e}\displaystyle\int_0^T \sigma_I^2(t)dt} \tag{8}$$

$$\eta_r = \frac{E_R}{E_I} = \frac{\dfrac{A_e}{\rho_e C_e}\displaystyle\int_0^T \sigma_R^2(t)dt}{\dfrac{A_e}{\rho_e C_e}\displaystyle\int_0^T \sigma_I^2(t)dt} \tag{9}$$

$$\eta_t = \frac{E_T}{E_I} = \frac{\dfrac{A_e}{\rho_e C_e}\displaystyle\int_0^T \sigma_I^2(t)dt}{\dfrac{A_e}{\rho_e C_e}\displaystyle\int_0^T \sigma_I^2(t)dt} \tag{10}$$

where η_a, η_r, and η_t are the energy dissipation rate, energy reflectance, and energy transmittance, respectively.

According to the calculation method for each energy component during the dynamic load impact process, Table 3 presents the energy of each component and its proportion under various conditions, comparing the same temperature with different cycle times and the same cycle times with different temperatures.

3.2.2. Analysis of the change of energy of each component with the number of cycles

From the energy calculation results of the two specimen processing methods, it is evident that the energy loss and absorption differ, showing distinct patterns. Figs. 10 and 11 display the change curves of each energy reflectance under different cycle times and temperatures.

In Fig. 10, it is observed that the energy reflectance and energy dissipation rate of the specimen gradually increase with the number of cycles, while the energy transmittance decreases. This pattern is attributed to the different degrees of damage inflicted on the specimens heated at the same temperature after varying cycle times. Physically, at 500 and 600 °C, visible surface cracks appeared after five cycles, becoming more distributed and deeper with up to seven cycles.

Analyzing the stress wave propagation during impact, the specimen undergoes different stages of crack formation. In Stage 1 (closed Micro-cracks), microcracks are mainly closed after 1 to 3 cycles. As the stress wave transmits from the incident rod, the small number of free surfaces result in less reflection and more forward transmission of energy. In Stage 2 (Open and closing cracks), with increased cycles (5–7), cracks expand, forming macro cracks with free surfaces. During impact, these cracks reflect the incident waves more significantly, consuming more energy. The incident stress wave transmits through reclosed cracks, resulting in higher reflection rates and increased energy consumption [25].

Thus, as cycle numbers increase, internal specimen damage exacerbates, leading to more crack formation and greater energy consumption. Consequently, the energy reflectance and dissipation rates rise, while energy transmittance decreases.

3.2.3. Analysis of energy changes of each component with temperature

Fig. 11 shows that with rising temperatures, the energy reflectance and dissipation rates increase, while energy transmittance decreases. The energy rate changes under varying temperatures but consistent cycle numbers mirror those observed with changing cycle numbers at consistent temperatures. Higher temperatures intensify internal crack development, resulting in the greater reflection and less transmission of stress waves.

Temperature changes significantly affect the energy components of the sandstone specimen. For example, between 500 and 600 °C, the difference in energy ratio is about 6–10 times greater than that between 200 and 500 °C. This suggests a critical temperature threshold at 500–600 °C. Below this threshold, temperature impact on specimen damage is less pronounced, while above it, damage increases exponentially.

In conclusion, the study of energy changes in sandstone under dynamic loading reveals that both the number of cycles and temperature significantly influence the specimen's energy reflectance, transmittance, and dissipation rates. As the number of cycles and temperature increase,

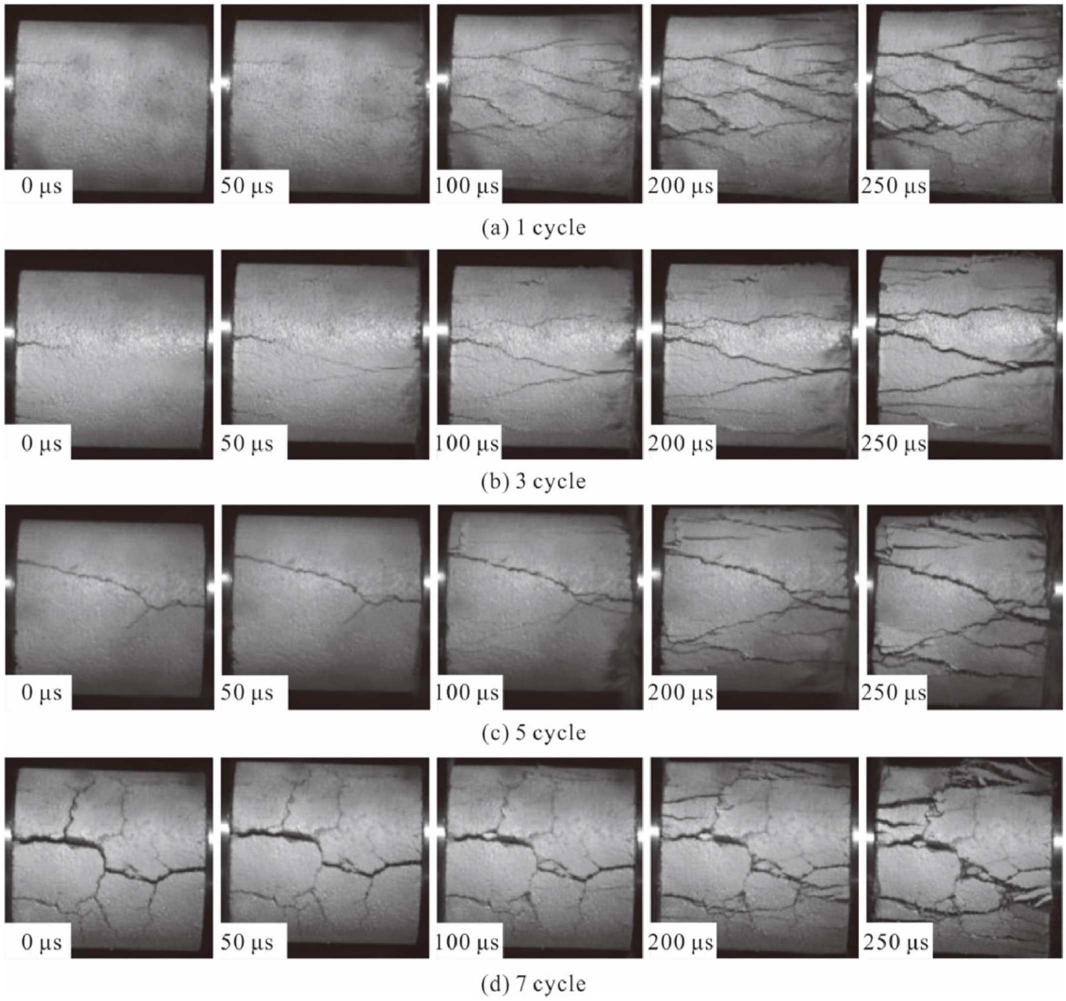

Fig. 12. Crack propagation of dynamic compression of sandstone at 600 °C.

internal damage and crack formation intensify, leading to greater energy reflection and dissipation, and reduced transmission, highlighting a critical threshold around 500–600 °C where the damage to sandstone becomes exponentially severe.

3.3. *Characterisation of crack expansion and damage patterns*

3.3.1. *Analysis of crack development with the number of cycles*

In the dynamic impact test of sandstone after high temperature-water cooling cycles, a high-speed camera was used to capture the damage process. The test, with a resolution of 256 × 256 and a frame rate of 40000 fps, focused on the crack expansion of sandstone specimens heated to 600 °C under different high temperature-water cooling cycles.

Fig. 12 shows the crack expansion of specimens from 0 to 250 μs after various cycles at 600 °C. The macro cracks on the specimen surface and their development increase with the number of cycles, resulting in wider cracks. Initially, at 50 μs, sandstone powder and small cracks appear on the specimen surface after 1 to 5 cycles. After 7 cycles, transverse cracks on the surface become compressed, and no further crack propagation is observed.

At 100 μs, cracks begin to connect and form axial cracks. After 1 to 3 cycles, the number of cracks increases significantly, forming through axial cracks. By the 5th cycle, these cracks connect with the original axial cracks, and after the 7th cycle, tiny cracks and some sandstone powder become visible.

At 200 μs, the cracking intensifies, forming main cracks through the specimens. By 250 μs, the specimens are damaged by multiple cracks, and broken rock masses start ejecting outwards.

The damage and crack distribution are closely related to the number of cycles. After 1 to 3 cycles, the damage is minor, with cracks primarily developing axially. After 5 to 7 cycles, the damage is more severe, with cracks forming through the axial direction, leading to compression-shear damage under impact load.

The increase in the number of cycles exacerbates internal microcrack formation due to dehydration, phase changes, and thermal fatigue, which results in macro crack expansion. Low cycle numbers cause tensile damage along the axial direction, while higher cycle numbers cause more severe internal damage, leading to an increase in cracks and compression-shear damage.

3.3.2. *Analysis of crack development with temperature change*

Fig. 13 shows the crack extension of sandstone under impact after 7 high temperature-water cooling cycles, heating the specimens to 200–600 °C. At 50 μs, microcracks and sandstone powder appear on the surface of all specimens. At 100 μs, crack propagation and sandstone powder ejection increase with temperature.

By 200 μs, cracks develop along the original cracks, while by 250 μs, the specimens are damaged, with broken rock pieces ejecting outwards. The higher the temperature, the more severe the damage and the greater the number of cracks, leading to more broken rock pieces.

At lower temperatures (200–400 °C), tensile cracks parallel to the axis are predominant. As the temperature increases, non-parallel cracks increase, and at 500–600 °C, intersecting cracks lead to compression-shear damage.

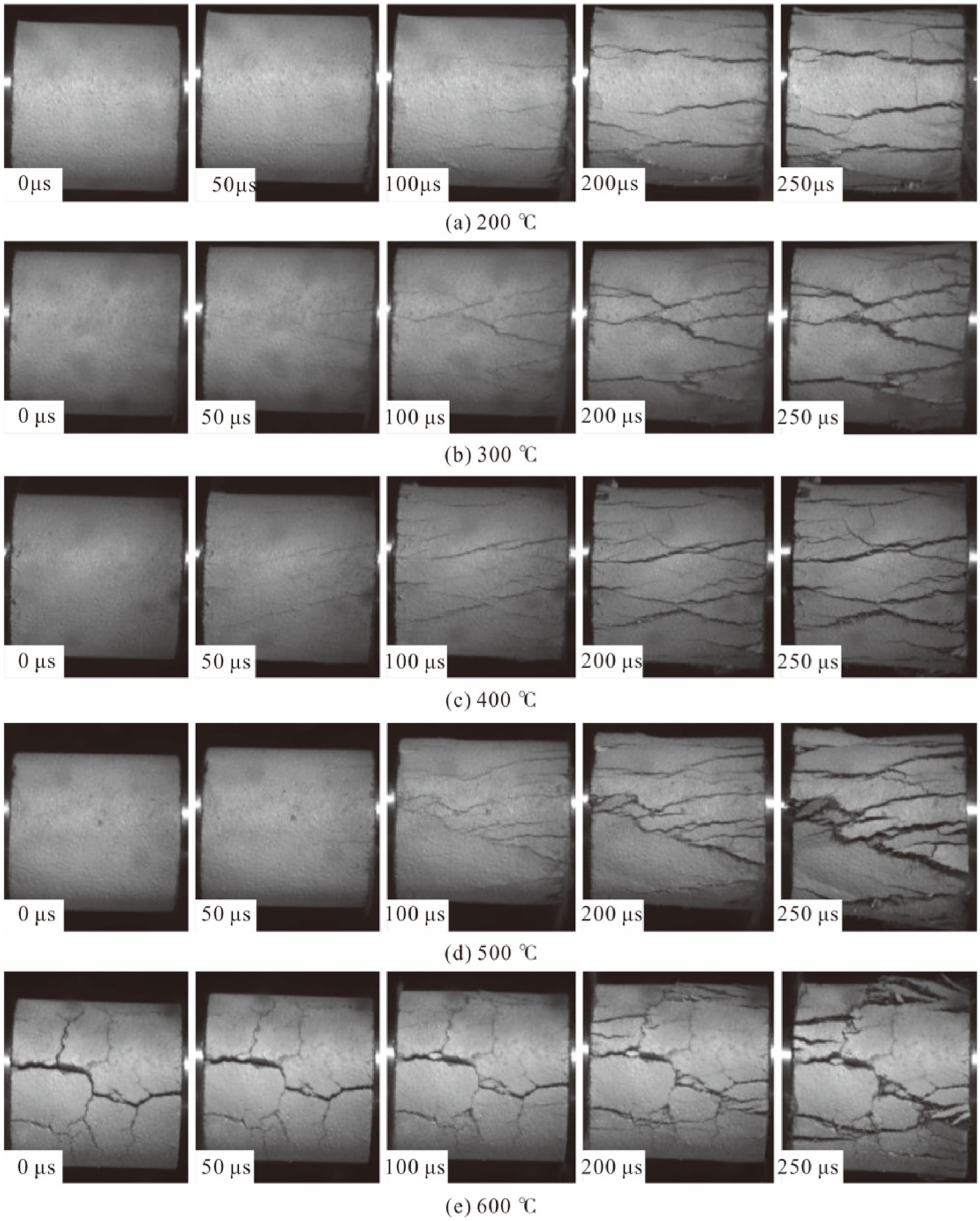

Fig. 13. Crack propagation of sandstone under dynamic compression under 7 cycle.

The increase in temperature causes thermal instability, dehydration, and phase transformation of minerals, resulting in microcracks. These microcracks reduce compressive and tensile strength, making the rock more susceptible to macro cracks and compression-shear damage under impact load. Thus, higher temperatures lead to more significant microscopic damage, increase crack numbers, and a transformation in damage forms.

3.3.3. Discussion of microscopic damage mechanism

The reduction in sandstone strength after high temperature treatment is due to changes in cement and other mineral phases. Different minerals have varying temperature sensitivities, leading to changes in cement content and mineral phase transformation at different temperatures. Cement, as the main load-bearing material, directly affects sandstone strength. High temperatures cause free water, crystalline water

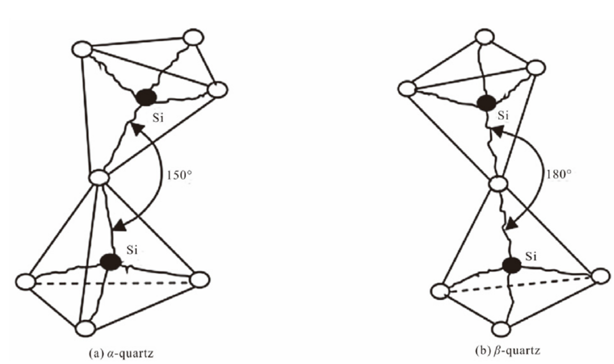

Fig. 14. Change sketch map of α-β quartz bond angle.

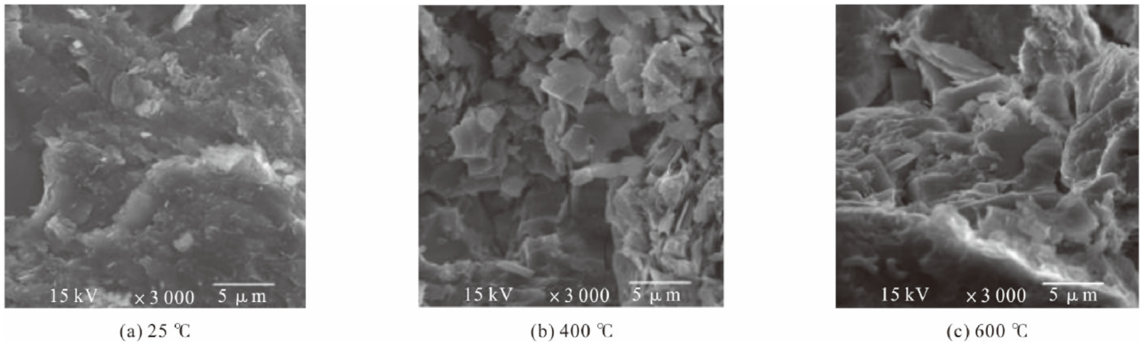

Fig. 15. Scanning electron microscope.

gasification, and escape, leading to pore space damage and strength reduction.

From a mineral composition perspective, Su et al. [26] conducted X-ray diffraction analysis on high-temperature sandstone and found that below 400 °C, kaolin disappears, the contents of other minerals decrease, and new substances such as calcium feldspar forms. The strength of sandstone initially increases with rising temperature due to an increase in quartz content but decreases significantly at 600 °C as quartz content drops.

Scanning Electron Microscope (SEM) analysis of high temperature sandstone reveals a few microcracks at 400 °C, and at 600 °C, fusion and recrystallisation further decrease strength. The transition of quartz from α-phase at room temperature to β-phase at higher temperatures causes an increase in crystal volume, leading to microcracks. The incomplete transition back to α-phase upon cooling causes tensile stress between quartz crystals and other mineral components, leading to cracks when tensile stress exceeds thermal stress.

Fig. 14 shows the change in bond angles between α-quartz and β-quartz, while Fig. 15 presents electron microscope scans of high-temperature sandstone.

In summary, higher temperatures exacerbate internal micro-damage and reduce tensile and shear resistance, leading to more cracks and a shift in damage form. The increase in temperature directly influences microcrack formation, affecting macroscopic damage evolution.

4. Conclusions

The influence of high-temperature water-cooling cycles on the dynamic behavior of sandstone has significant implications for the safety and stability of geothermal energy extraction processes. Understanding these influences is critical for preventing geological disasters such as rock bursts, induced seismicity, and structural failures. Based on the dynamic impact tests of sandstone after high-temperature water-cooling cycles, and through the analysis of dynamic strength, energy components during impact, and crack propagation, the following conclusions were drawn:

(1) The compaction and elasticity phases of the specimens at 200–500 °C are extremely short and remain so with increasing temperature and cycle number. At 600 °C, with increasing cycles, these phases significantly lengthen. This change occurs as macroscopic cracks form parallel to the specimen's cross-section during the high-temperature water-cooling cycle, leading to an increase in compression and elasticity stages prior to impact.

(2) With increased cycles and heating temperature, peak dynamic stress decreases while dynamic strain increases. At 500–600 °C, there exists a critical temperature where dynamic stress rapidly decreases and dynamic strain sharply rises, indicating a significant weakening of the specimen's resistance to impact deformation and resulting in severe damage.

(3) Peak dynamic compressive strength declines with rising temperature and cycle counts, while dynamic strain trends upward. For specimens at 200–600 °C, the reduction in dynamic peak stress from 1 to 7 cycles is 3.4%, 4.3%, 4.6%, 10.5%, and 42.3%, respectively. The amplitude of dynamic stress reduction from 1 to 7 cycles is 16.9%, 16.0%, 9.7%, and 55.3%.

(4) Energy reflectivity and energy dissipation increase with higher temperatures and more cycles, while energy transmittance decreases. Particularly above 500 °C, the differences in energy ratios grow significantly, indicating a temperature threshold beyond which specimen damage escalates exponentially.

(5) High-speed camera analysis of crack extension reveals that increased cycles and temperature exacerbate microscopic damage, altering the crack evolution pattern. This leads to a reduction in the rock's tensile shear capacity and a shift in the predominant form of damage from tensile to compression-shear damage.

CRediT authorship contribution statement

Lei Hong: Writing – review & editing, Writing – original draft, Validation, Software, Methodology, Investigation, Formal analysis, Data curation. **Wen Wang:** Supervision, Project administration, Funding acquisition, Data curation, Conceptualization. **Xuewen Cao:** Writing – review & editing, Writing – original draft, Visualization, Validation, Supervision, Software, Methodology, Investigation, Formal analysis, Data curation. **Yuxiang Song:** Supervision, Formal analysis, Data curation. **XiaoWei Lu:** Supervision, Software, Resources. **Shu Jiang:** Software. **Cheng Zhai:** Resources.

Declaration of conflict of interest

The authors declare no conflicts of interest regarding the publication of this article.

Acknowledgements

Thanks to the support by the National Natural Science Foundation of China (No. 52174109); Henan University Science and Technology Innovation Talent Programme (No. 23HASTIT011); research and development of key technologies and complete sets of equipment for safe cooperative exploitation of natural gas, coal and uranium resources, Henan Province key research and development project (No. 241111320800); 2023 Safety Discipline "Double First-Class" Construction Project, Cultivation Category: Major Technological Breakthroughs (No. AQ20230501); and 2023 Basic Research Business Fund Special Project, National Major Achievement Cultivation, Theory and Key Technologies for the Cooperative Exploitation of Natural Gas and Coal Resources.

References

[1] J. Xu, S. Luo, X. Xiao, Review of the experimental studies of the cracking behaviors of fractured rocks under compression, Geohazard Mech. 2 (2) (2024) 59–82.

[2] A.P. Khmelinin, A.I. Konurin, E.V. Denisova, Simulation of electromagnetic high-frequency wave propagation processes in multilayer geo-structures, Geohazard Mech. 1 (3) (2023) 203–207.

[3] K. Li, C. Qi, M. Wang, J. Li, H. Chen, Research on the influence of rock fracture toughness of layered formations on the hydraulic fracture propagation at the initial stage, Geohazard Mech. 2 (2) (2024) 121–130.

[4] W.G.P. Kumari, P.G. Ranjith, M.S.A. Perera, B.K. Chen, I.M. Abdulagatov, Temperature-dependent mechanical behaviour of Australian Strathbogie granite with different cooling treatments, Eng. Geol. 229 (2017) 31–44.

[5] W.G.P. Kumari, P.G. Ranjith, M.S.A. Perera, B.K. Chen, Experimental investigation of quenching effect on mechanical, microstructural and flow characteristics of reservoir rocks: thermal stimulation method for geothermal energy extraction, J. Petrol. Sci. Eng. 162 (2018) 419–433.

[6] M. Liang, S. Zhang, B. Shu, Influence of different cooling methods on the splitting characteristics of high-temperature granite in Brazil, J. Water Resour. Water Eng. 29 (2) (2018) 186–193.

[7] Z. Huang, Y. Zhang, W. Wu, Mechanical and fluctuation characterisation of high-temperature marble cooled by water, Geotechnics 37 (2) (2016) 367–375.

[8] T. Yin, X. Li, W. Cao, K.W. Xia, Effects of thermal treatment on tensile strength of Laurentian granite using Brazilian test, Rock Mech. Rock Eng. 48 (6) (2015) 2213–2223.

[9] L. Yu, H. Peng, G. Li, Y. Zhang, Z. Han, H. Zhu, Experimental study on granite under high temperature-water cooling cycle, Geotechnics 42 (4) (2021) 1025–1035.

[10] Y. Li, E. Zhai, Z. Zhang, Q. Peng, Q. Yang, Effect of high temperature heating-water cooling cycle on the physical and mechanical properties of granite, China High-Tech (8) (2021) 67–70.

[11] Y. Yu, Y. Zhao, Experimental study on the mechanical properties of granite cooled by water at high temperature within 600 °C, J. Rock Mech. Eng. 29 (5) (2010) 892–898.

[12] H. Wang, Z. Wang, C. Xiong, L. Cheng, S. Zhan, Experimental study on radial compression mechanical characteristics of circular granite under warm and wet cycling conditions, J. Rock Mech. Eng. 39 (S2) (2020) 3260–3270.

[13] T. Yin, X. Li, Z. Zhou, L. Hong, Z. Ye, Study on dynamic mechanical properties of siltstone after high temperature, J. Undergr. Spac. Eng. (6) (2007) 1060–1063.

[14] Y. Yu, Q. Xu, X. Diao, Z. Yan, Influence of cyclic impact on the characteristics of sandstone under peripheral pressure, J. Huazhong Univ. Sci. Technol. 47 (6) (2019) 127–132.

[15] D. Li, X. Sun, Z. Zhou, X. Cai, G. Qiu, Dynamic cumulative damage characteristics of granite under multiple impact loads, Exp. Mech. 31 (6) (2016) 827–835.

[16] D. Lin, S. Chen, Experimental study on the damage law of rock under cyclic impact loading, J. Rock Mech. Eng. (22) (2005) 4094–4098.

[17] Q. Ping, Q. Ma, P. Yuan, Analysis of energy dissipation in SHPB splitting tensile test of rock specimens, J. Min. Saf. Eng. 30 (3) (2013) 401–407.

[18] B. Dai, X. Luo, Q. Sin, Y. Chen, Y. Liu, Analysis of damage characteristics and energy dissipation of rocks with holes under cyclic impact loading, Chinese J. Saf. Sci. 30 (7) (2020) 69–77.

[19] J. Zhu, X. Li, F. Guang, S. Wang, Dynamic characteristics of rocks under uniaxial cyclic impact and its damage modelling, J. Geotech. Eng 35 (3) (2013) 531–539.

[20] T. Wang, Z. Song, J. Yang, Dynamic response characteristics of weathered red sandstone under cyclic impact, J. Rock Mech. Eng. 38 (S1) (2019) 2772–2778.

[21] W. Zhang, B. Shi, Z. Mu, Experimental study of coal rock crushing and energy dissipation law under impact load, J. Min. Saf. Eng. 33 (2) (2016) 375–380.

[22] W. Wang, H. Li, H. Gu, Experimental study on strength characteristics of water-bearing coal samples loaded by three-dimensional dynamic-static combination, J. Rock Mech. Eng. 36 (10) (2017) 2406–2414.

[23] W. Wang, H. Li, R. Yuan, Mechanical characteristics and fine mechanical analysis of water-bearing coal samples loaded by dynamic-static combination, J. Coal 41 (3) (2016) 611–617.

[24] W. Wang, Y. Wu, X. Lu, G. Zhang, Study on small coal pillar in gob-side entry driving and control technology of the surrounding rock in a high-stress roadway, Front. Earth Sci. 10 (2023) 1020866.

[25] Q. Zheng, Mechanical Properties and Fracture Characteristics of Damaged Sandstone under Dynamic Loading, Anhui University of Technology, 2021.

[26] C. Su, S. Wei, B. Qin, Y. Yang, Experimental study on the influence mechanism of high temperature on mechanical properties of fine sandstone, Geotechnics 38 (3) (2017) 623–630.